Cable Modeling for Very Fast Transient Simulation Studies Using One-Sided Voltage Transfer Function Measurements

Bjørn Gustavsen, *Fellow*, *IEEE*

***Abstract*—A novel measurement-based method for high-frequency modeling of shielded cables is introduced for use in very fast transient simulation studies. The method requires measurements on one cable end only, thereby being applicable to installed cable systems. Three frequency sweep voltage transfer measurements are performed at one cable end using a vector network analyzer (VNA) with gain-phase setup, two voltage probes and one series resistor. From the measurements is calculated the cable 2×2 admittance matrix as function of frequency where a sign arbitrariness is removed using a local rational model that is swept along the frequency samples. The resulting admittance matrix can be fitted by a lumped-parameter rational model, or be subjected to modeling by a frequency-dependent traveling wave model which also permits to change the cable length. Application to a 150 mm^2 single core cable of 252 m length demonstrates that the model reproduces measured cable high-frequency damping effects that result in sub-microsecond voltage rise times. A classical modeling approach based on skin effect formulae gives too little damping.**

***Index Terms*—Cable, very fast transients, modeling, simulation.**

I. Introduction

VERY fast transient (VFT) overvoltages can lead to excessive internal voltage stresses in machines and transformers due to non-linear voltage distributions along the windings [1], [2]. The operation of circuit breakers and disconnectors are typical sources of such overvoltages [1], in addition to switch-mode power electronic converters [3]. The accurate modeling of cables is essential in prediction of the resulting overvoltage stresses, e.g. when a motor is fed from a variable speed drive through a cable.

Electromagnetic transient (EMT) programs have built-in support routines that can produce frequency-dependent traveling wave models of typical cable designs [4], [5]. The input parameters of these models are obtained by evaluating a set of analytical expressions that consider the skin effect in conductors [6], [7] and in some instance also proximity effects [8], while the partial capacitances are calculated assuming lossless permittivities. The accuracy of the input parameters and thus the resulting cable model tends to deteriorate at high frequencies due to the assumption of perfectly round or tubular conductors, and due to the assumption of lossless insulation and semiconductor layers. Even with the use of finite element method (FEM) calculations [9],[10], the accurate calculation of the cable response is difficult at very high frequencies [11].

The accuracy problem can be overcome by characterizing the cable behavior using small-signal measurements in the frequency domain, from which a frequency-dependent model can be extracted via rational function approximation. The works in [12] and [13] describe methodologies where scattering (S-) parameter measurements are performed using both cable ends to obtain parameters that characterize the behavior of a frequency-dependent multi-conductor cable, and to extract per-unit-length (p.u.l.) parameters [13]. Another approach is to measure the cable terminal admittance directly using the approach in [14] or via the two-probe measurement approach described in the Appendix of [15], but again both cable ends must be accessible.

In what follows is proposed an alternative approach which only requires measurement access to one cable end, thereby being applicable to installed cables. The method is suitable for modeling systems of parallel coaxial type cables provided that 1) the metallic screens are grounded at both ends with a low-impedance grounding, and 2) that there are no cross-bondings. This includes typical high-voltage single-core and three-core cables. High-frequency wave propagation on such cable systems takes place in the form of coaxial waves between the cable conductors and associated screens, implying that there is virtually no coupling between the cables or to nearby objects. Each cable can then be modelled as a single-conductor transmission line.

With these assumptions, the cable 2×2 terminal admittance matrix can be obtained using a voltage transfer function measurement on one cable end with the opposite cable end open and shorted. In addition, a third measurement is used for probe calibration. The three measurements are performed in the frequency domain using a vector network-analyzer (VNA) with

Manuscript received… This work was supported by the consortium participants of the SINTEF-led project "FastTrans" (project no. 294508/E20).

B. Gustavsen is with SINTEF Energy Research, N-7465 Trondheim, Norway (e-mail: bjorn.gustavsen@sintef.no).

gain-phase setup in combination with two passive voltage probes and a series resistor. The calculation of the admittance matrix is shown to give a sign arbitrariness in the off-diagonal element. The correct sign is determined by fitting a local rational model to the off-diagonal element in the form of a sliding window. Two alternative simulation models are extracted from the terminal admittance, a lumped parameter model and a traveling wave model. The method is demonstrated for a 252-m single core cable where a steep-fronted voltage is applied to one cable end. The simulated result for the far end voltage and near end current is compared with a direct measurement and with the result obtained by the conventional modeling approach used in EMT programs.

II. Problem Statement

Consider a single-conductor homogenous transmission line. The terminal behavior with respect to ends 1 and 2 can be described in terms of frequency domain impedance parameters (1) or admittance parameters (2). In both representations, the diagonal and off-diagonal elements are pairs of identical elements, due to the homogenous condition.

$$\begin{bmatrix} V_1(\omega) \\ V_2(\omega) \end{bmatrix} = \begin{bmatrix} Z_a(\omega) & Z_b(\omega) \\ Z_b(\omega) & Z_a(\omega) \end{bmatrix} \cdot \begin{bmatrix} I_1(\omega) \\ I_2(\omega) \end{bmatrix} \tag{1}$$

$$\begin{bmatrix} I_1(\omega) \\ I_2(\omega) \end{bmatrix} = \begin{bmatrix} Y_a(\omega) & Y_b(\omega) \\ Y_b(\omega) & Y_a(\omega) \end{bmatrix} \cdot \begin{bmatrix} V_1(\omega) \\ V_2(\omega) \end{bmatrix} \tag{2}$$

Our objective is to obtain the matrix elements of (2) by measurements. The two cable ends may be physically far apart so that it is not possible to simultaneously perform a measurement at both ends. We therefore consider it a requirement that the necessary measurements can be performed at one cable end only. Finally, the admittance elements are to be subjected to model extraction to obtain a model compatible with EMT simulation programs for transient simulation studies.

III. Measurement Principle

A. Terminal Conditions

The cable is at the near end fed from a voltage source as shown in Fig. 1. Two alternative conditions are considered for the far end: a) open-ended, and b) short-circuited to ground, i.e. to the metallic screen.

B. Open Condition

In this case we have $I_2 = 0$. From (1) we get $V_1 = Z_a I_1$ so that

$$Z_a = \frac{V_1^{\text{open}}}{I_1^{\text{open}}} \tag{3}$$

This implies that Z_a in (1) can be obtained by measuring V_1 and I_1 in the open circuit condition.

C. Shorted Condition

In this case we have $V_2 = 0$. From (2) we get $I_1 = Y_a V_1$ so that

$$Y_a = \frac{I_1^{\text{short}}}{V_1^{\text{short}}} \tag{4}$$

This implies that Y_a can be obtained by measuring V_1 and I_1 in the short-circuit condition.

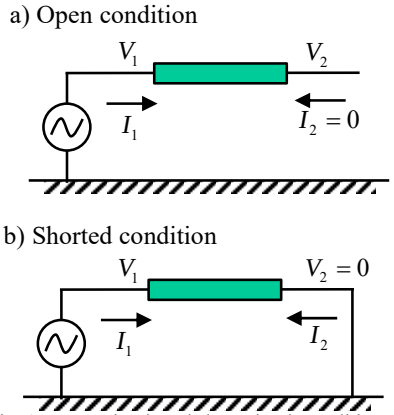

Fig. 1. Open-circuit and short-circuit condition.

D. Calculating Off-Diagonal Term Y_b

The inverse of the admittance matrix (2) has the analytical solution

$$\begin{bmatrix} Y_a & Y_b \\ Y_b & Y_a \end{bmatrix}^{-1} = \frac{1}{Y_a^2 - Y_b^2} \begin{bmatrix} Y_a & -Y_b \\ -Y_b & Y_a \end{bmatrix} = \begin{bmatrix} Z_a & Z_b \\ Z_b & Z_a \end{bmatrix} \tag{5}$$

We therefore have

$$Z_a = \frac{Y_a}{Y_a^2 - Y_b^2} \tag{6}$$

Solving (6) for Y_b gives

$$Y_b = \pm \sqrt{Y_a^2 - \frac{Y_a}{Z_a}} \tag{7}$$

With Y_a and Y_b obtained from (4) and (7), all elements of the admittance matrix in (2) have been determined.

IV. Correcting Sign of Admittance Off-Diagonal Term

The sign of Y_b in (7) as returned by any calculation program is in principle arbitrary. The following describes a procedure that is used for removing sign errors.

A. Low-Frequency Samples

It is assumed that the lowermost frequency samples are at frequencies much lower than the first resonance point. At such frequencies, the real and imaginary part of Y_b must respectively be negative and positive, and the sign of the low-frequency samples can therefore easily be corrected.

B. Remaining Samples

A sliding window is defined that uses a fixed number of contiguous sub-samples of Y_b. The samples within the window are fitted with a low-order rational function with poles in the left half plane, using vector fitting [17]. The poles and residues

are real or complex conjugate. From the rational function, the real and imaginary part of Y_b are calculated at the first out-of-band sample $K+1$. This predicted sample value $\overline{Y}_b(\omega_{K+1})$ is compared with the calculated sample $Y_b(\omega_{K+1})$ by (7). The sign of $Y_b(\omega_{K+1})$ is chosen such that $\| Y_b(\omega_{K+1}) - \overline{Y}_b(\omega_{K+1}) \|$ is minimum. After selecting the sign of the next sample, the sliding window is shifted one sample towards higher frequencies, and the procedure is repeated until all samples have been processed. The sliding window therefore includes a fixed number of samples that are repeatedly shifted by a single frequency step.

Fig. 2 shows an example demonstrating the sign correction procedure on the imaginary part of Y_b. (The example has 21 frequency samples in the window and uses a 6th order rational approximation). It is observed that the rational model provides the correct sign of Y_b at the next frequency sample.

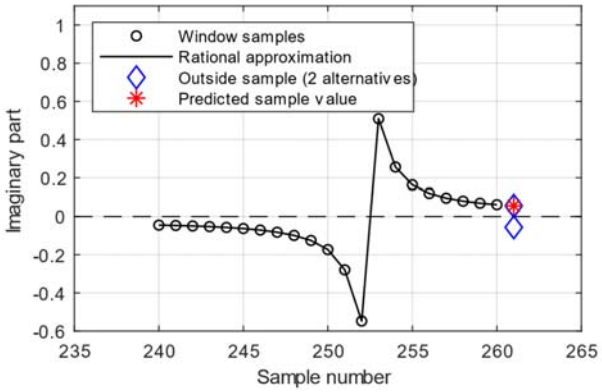

Fig. 2. Selecting sample value using rational function.

V. Measurement Setup And Procedure

The frequency domain measurements are performed using a vector network analyzer (VNA) with gain-phase setup in combination with two high-impedance (10 MΩ) passive voltage probes, see Fig. 3. The series resistor R is placed between the VNA output (S) and the cable conductor. The two probes are connected to the VNA reference (R) and input (T) terminals which have 1 MΩ input impedance. Using the VNA, the voltage ratio $h = v_T / v_R$ is measured as function of frequency over a band of frequencies specified by the operator.

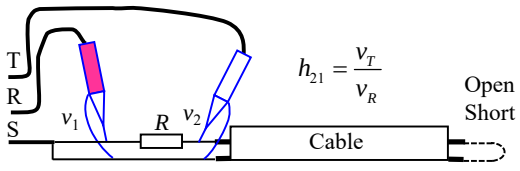

Fig. 3. Voltage transfer measurements.

The impedance seen into the cable can now be measured as

$$Z = \frac{v_2}{i} = \frac{R \cdot v_2}{v_1 - v_2} = \frac{R \cdot h_{21}}{1 - h_{21}} \quad , h_{21} = \frac{v_2}{v_1} \tag{8}$$

The measurement is performed with two alternative cable terminations as shown in Table I. The two measurements give Z_a and Y_a by (9) and (10) from which Y_b is obtained by (7).

TABLE I
MEASUREMENTS

Measurement	Quantity	Cable end condition
1	$h_{21}^{\text{open}} = v_T / v_R$	Open
2	$h_{21}^{\text{short}} = v_T / v_R$	Shorted

$$Z_a = Z^{\text{open}} = \frac{R \cdot h_{21}^{\text{open}}}{1 - h_{21}^{\text{open}}} \tag{9}$$

$$Y_a = (Z^{\text{short}})^{-1} = \frac{1 - h_{21}^{\text{short}}}{R \cdot h_{21}^{\text{short}}} \tag{10}$$

The measurements do not require the two voltage probes to be identical or to be matching the input impedance of the VNA. Any difference in probe frequency response is handled by the use of a probe calibration factor $V_{\text{cal}}(\omega) = (v_T / v_R)^{-1}$ that is obtained by a third, separate measurement with the two probe tips connected and the two probe grounding clips connected. The probe calibration factor V_{cal} is introduced as a scaling factor for h_{21} in (8), $h_{21} \rightarrow V_{\text{cal}} \cdot h_{21}$.

VI. Model Extraction for Time Domain Simulation

A. Lumped Parameter Modeling

From the measured admittance matrix (2), a pole-residue type rational model is calculated,

$$\mathbf{Y}^{2\times2}(\omega) \approx \mathbf{R}_0^{2\times2} + \sum_{i=1}^{N} \frac{\mathbf{R}_i^{2\times2}}{j\omega - a_i} \tag{11}$$

The rational model (11) can be calculated by direct application of vector fitting [17] and subsequent passivity enforcement by e.g. residue perturbation [18], [19]. Unfortunately, with such direct fitting approach the information about charging currents tend to become lost towards lower frequencies. This problem is avoided by noting that the 2×2 admittance matrix (2) can be exactly diagonalized by the frequency-independent transformation

$$\mathbf{T}^{-1}\,\mathbf{Y}^{2\times2}(\omega)\mathbf{T} = \begin{bmatrix} \lambda_1^Y(\omega) & 0 \\ 0 & \lambda_2^Y(\omega) \end{bmatrix}, \mathbf{T} = \frac{1}{\sqrt{2}}\begin{bmatrix} 1 & 1 \\ 1 & -1 \end{bmatrix} \tag{12}$$

We can therefore independently fit the two eigenvalues with a passive rational model,

$$\lambda_j^Y \approx r_{0,j} + \sum_{i=1}^{N_j} \frac{r_{i,j}}{j\omega - a_{i,j}}, \; j = 1,2 \tag{13}$$

For use in time domain simulations, the model can be used on its diagonal form (12), (13), or it can be converted into the phase domain (14).

$$\mathbf{Y}^{2\times2}(\omega) \approx \mathbf{R}_{0,1}^{2\times2} + \mathbf{R}_{0,2}^{2\times2} + \sum_{i=1}^{N_1} \frac{\mathbf{R}_{i,1}^{2\times2}}{j\omega - a_{i,1}} + \sum_{i=1}^{N_2} \frac{\mathbf{R}_{i,2}^{2\times2}}{j\omega - a_{i,2}} \tag{14}$$

where

$$\mathbf{R}_{i,1}^{2\times 2} = \mathbf{T}\begin{bmatrix} r_{i,1} & 0 \\ 0 & 0 \end{bmatrix}\mathbf{T}^{-1} \quad ,i = 0,\ldots,N_1 \tag{15a}$$

$$\mathbf{R}_{i,2}^{2\times 2} = \mathbf{T}\begin{bmatrix} 0 & 0 \\ 0 & r_{i,1} \end{bmatrix}\mathbf{T}^{-1} \quad ,i = 0,\ldots,N_2 \tag{15b}$$

The model (14) can be directly converted into a state-space model for use in EMTP or PSCAD, or be converted into a RLC network for use with ATP [20]. In the example in this work (Section IX), the simulations are performed in the Matlab environment using time domain discretization of the associated ordinary differential equations. The procedure is described in detail in [21] which includes link to downloadable code.

B. Traveling Wave Modeling

The cable p.u.l. parameters of series impedance Z_s and shunt admittance Y_s are calculated from Y_a and Y_b using a procedure described in [13]. The approach is repeated here, for convenience.

The relation between p.u.l. parameters and admittance matrix elements is given by (16a) and (16b) [23] where Y_C is the cable characteristic admittance, γ is the propagation constant, and d is the cable length.

$$Y_a = Y_C \coth(d\gamma) \tag{16a}$$

$$Y_b = \frac{-Y_C}{\sinh(d\gamma)} \tag{16b}$$

Combining (16a) with (16b) allows to calculate $d\gamma$,

$$d\gamma = \cosh^{-1}(-Y_a / Y_b) + j2\pi i \tag{17}$$

With $d\gamma$ known, the p.u.l. series admittance Y_s is calculated by (18a). The expression results from (16b) when introducing the relations $\gamma^2 = Z_s Y_s$ and $Y_C = \sqrt{Y_s / Z_s}$. Finally, the p.u.l. series impedance Z_s is calculated by (18b).

$$Y_s = -Y_b \gamma \sinh(d\gamma) \tag{18a}$$

$$Z_s = \frac{\gamma^2}{Y_s} \tag{18b}$$

The integer value i in (17) is a result of a sign arbitrariness in $\cosh^{-1}$ of complex numbers. The integer values are determined by requiring the imaginary part of $d\gamma$ to be a monotonously increasing function of frequency.

The obtained values $Y_s(\omega)$ and $Z_s(\omega)$ are used for calculating the cable propagation function $H(\omega)$ (19a) and characteristic admittance $Y_C(\omega)$ (19b), which are respectively fitted with a delayed and delay-less rational function. The two rational models in (19a)-(19b) define the parameters of a frequency-dependent traveling wave model which is compatible with most EMTP-type simulation programs.

$$H(\omega) = e^{-\sqrt{Y_s Z_s}\,d} \approx \left(\sum_{i=1}^{N_H} \frac{r_i^H}{j\omega - a_i^H}\right) e^{-j\omega\tau} \tag{19a}$$

$$Y_C(\omega) = \sqrt{\frac{Y_s(\omega)}{Z_s(\omega)}} \approx r_0^{Y_C} + \sum_{i=1}^{N_{Y_C}} \frac{r_i^{Y_C}}{j\omega - a_i^{Y_C}} \tag{19b}$$

It is observed that the length d appears as a parameter in H (19a). This implies that a cable model can in principle be calculated for any cable length.

VII. Example: Single Core Cable Modeling

A. Cable Object

The measurement and modeling procedure was applied to a 252 m cable on drum. It is a 12 kV fire resistant EPR cable with 150 mm^2 aluminum conductor and a 21 mm^2 double-layer braided screen. This cable type is often used in offshore applications. Fig. 4 shows the conductor cross-sectional area. The two screens were bonded together at both cable ends.

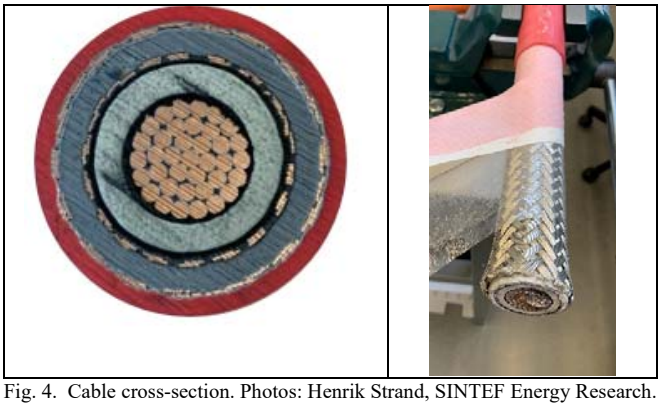

Fig. 4. Cable cross-section. Photos: Henrik Strand, SINTEF Energy Research.

B. Voltage Transfer Measurements

Voltage transfer functions h_{11} and h_{21} were measured with open and shorted conditions as described in Section VI, using a series resistor $R = 30\ \Omega$. The measurements were performed using a VNA (Agilent E5061B-3L5), giving 801 linearly spaced samples between 5 Hz and 15 MHz. In order to resolve the low-frequency behavior, an additional sample set was measured between 5 Hz and 5 MHz, using logarithmically spaced samples with 5 samples per decade of frequency.

C. Admittance Calculation

Y_a and Y_b were calculated from the measured h_{21}^{open} and h_{21}^{short} using (9), (10) and (7).

Fig. 5 shows the magnitude function of elements Y_a and Y_b. It is observed that the elements are characterized by a large number of evenly spaced resonances.

The sign of Y_b was corrected using the method described in Section IV. The sign correction used a 20-sample sliding window that was fitted by a 12$^{\text{th}}$ order rational model, requiring a total of 3.1 sec. Fig. 6 shows the result on the imaginary part of Y_b, in the range 100 kHz – 1 MHz.

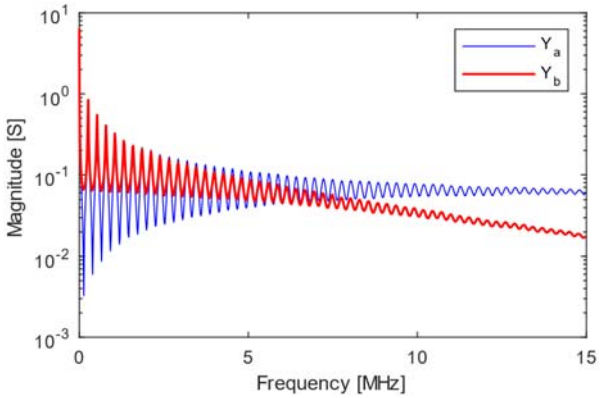

Fig. 5. Magnitude functions of elements Y_a and Y_b.

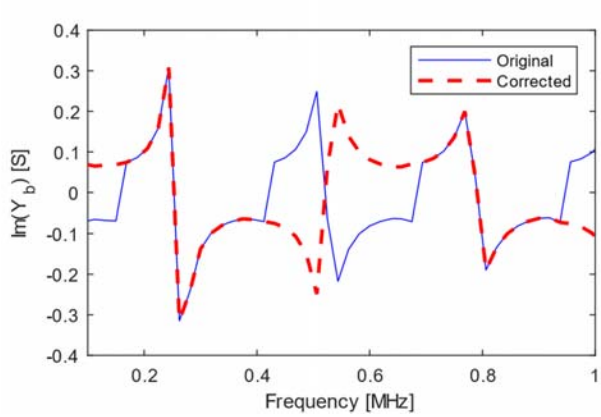

Fig. 6. Imaginary part of Y_b.

D. Lumped Parameter Model Extraction

The two eigenvalues λ_1^Y and λ_2^Y were fitted independently by vector fitting (VF) [17] with N=250 poles, giving a rational model (8) which was subjected to passivity enforcement using residue perturbation [19]. The rational approximation and the original data are shown in Fig. 7 for the differential mode. A similar accuracy was achieved for the common-mode eigenvalue. The fitting process by VF was achieved using 10 pole relocating iterations, requiring 3.8 sec for both eigenvalues.

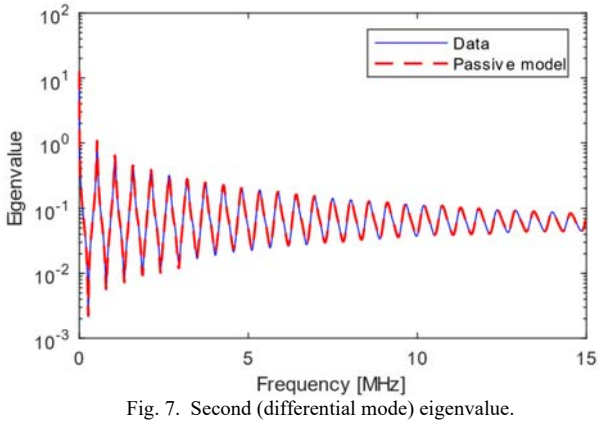

Fig. 7. Second (differential mode) eigenvalue.

E. Traveling Wave Model Extraction

Figs. 8a and 8b show the magnitude responses of H and Y_C together with a rational approximation using 10 and 8 poles, respectively. It is observed that while H is quite smooth and easily fitted, Y_C has some oscillations above 100 kHz. These oscillations are a consequence of inaccurate measurement of Y_a and Y_b as the magnitude function of Y_C is known to be a smooth function of frequency. The rational approximation was calculated using a prescribed set of real poles to obtain a fairly smooth response. Section XI.A discusses the effect of using a constant real-valued Y_C, indicated by the horizontal dashed line.

Passivity was verified by calculating the terminal admittance matrix $\mathbf{Y}$ (2) from the fitted H and Y_C using (20a) and (20b) [22]. It was verified that the real part of the (symmetrical) $\mathbf{Y}$ has positive eigenvalues at all frequencies, thereby complying with the passivity requirement.

$$Y_a = Y_C \frac{1+H^2}{1-H^2} \tag{20a}$$

$$Y_b = -2Y_C \frac{H}{1-H^2} \tag{20b}$$

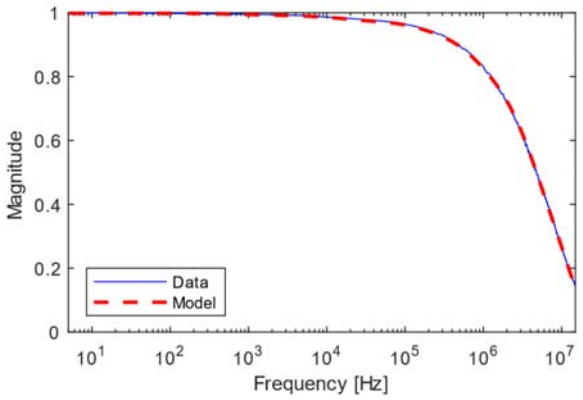

Fig. 8a. Propagation function H.

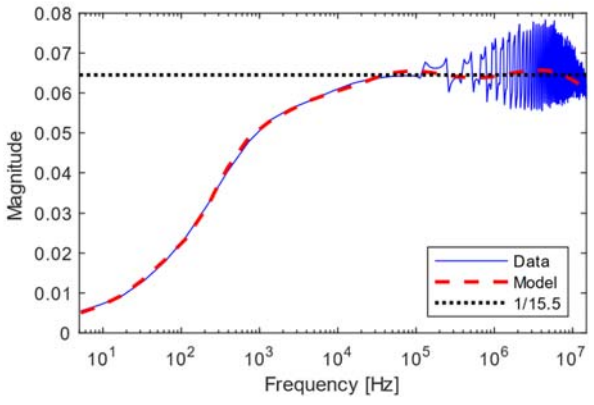

Fig. 8b. Characteristic admittance Y_C.

VIII. Modeling by Classical Method

The accuracy advantage of the proposed method becomes evident when comparing simulated results against those obtained using a "classical" modeling approach found in most EMTP-type programs.

The conductor is represented by a round, solid conductor

while the two wire screens are each represented by a tubular conductor. The conductivity of the two tubular conductors is calculated such that it gives a DC resistance equal to that of 8 mm^2 Cu, which is the specified effective copper area. The two semiconductor layers are in the series impedance calculations replaced with insulation because their conductivity is negligible compared to that of the adjacent metal [24]. In the shunt capacitance calculation, the two semiconductor layers are assumed to represent a short-circuit of the electric field. The entire space between the conductor and the inner metallic screen is replaced with an equivalent homogenous insulation with permittivity $\varepsilon_r = 3.57$ such that the conductor-screen capacitance matches that of the measured cable capacitance of the cable [24]. That way, the two semiconductive layers are effectively handled by replacing them with an insulating material. The cable geometry and conductor conductivities are listed in Table II, with d and t denoting diameter and thickness, respectively.

Using the cable data in Table II and the aforementioned considerations for semiconductive layers, the 3×3 cable series impedance is calculated in the frequency domain using the classical method [25], [7] which considers skin effect in conductors, while the 3×3 lossless capacitance matrix is calculated using the standard capacitance formula for cylindrical shells. This information is used to calculate parameters for the Universal Line Model [5], which is a frequency-dependent traveling wave model.

TABLE II
SINGLE-CORE CABLE DATA

Item	Property
Conductor	d=14.7 mm , σ=58·10^6 S/m
Inner semicon	t=0.9 mm
Insulation	t=3.54 mm
Outer semicon	t=0.9 mm
Inner wire screen	t=0.6 mm, σ=9.6·10^6 S/m
Insulation	t=5.0 mm, ε_r=2.3
Outer wire screen	t=0.6 mm, σ=6.7·10^6 S/m
Insulating jacket	t=2.1 mm, ε_r=2.3

IX. TIME DOMAIN VALIDATION

A. Measurements

The accuracy of the proposed modeling approach is validated by comparison against time domain measurements, see Fig. 9. The measurements utilized a function generator to produce a steep-fronted voltage, two voltage probes, a wide-band current sensor (Pearson model 4100), and a storage oscilloscope. The measurements were performed with the cable on drum, making both cable ends accessible by a single oscilloscope.

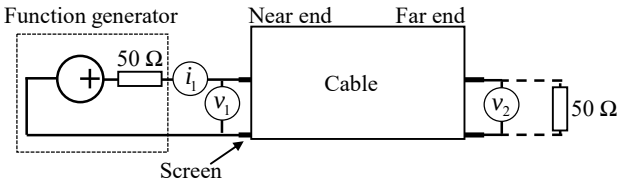

Fig. 9. Measurement of time domain voltage and current waveforms.

B. Open End

The function generator produced a step-like voltage on the near cable end with the far end open. The measured near end voltage $v_1(t)$ was applied to the alternative models as an ideal voltage source, and the models were used to simulate the far end voltage.

Fig. 10a shows the measured and simulated far end voltage v_2 using the lumped parameter model and the traveling wave model. Both models give an excellent reproduction of the measured waveform.

Fig. 10b shows a zoomed view which includes the first wave arrival at the far end. The far end voltage (v_2) has in the plot been shifted by 1.8 µs so that it can be directly compared with the near end voltage (v_1). The plot also includes the result by the classical modeling approach described in Section VIII. The proposed models gives an excellent reproduction of the measured wavefront while the classical model gives a wavefront with much too little damping. It is remarked that in the classical model the conductor-screen capacitance has been scaled by a factor of 0.87 in order to get a time delay which matches that of the measurement.

Fig. 10c compares the measured near end current with simulations. The errors are with both the lumped parameter model and the traveling wave model higher than in the voltage response measurement (Fig. 10a). The oscillation in the response by the lumped parameter model (after 20 µs) was found to be a result of the passivity enforcement step.

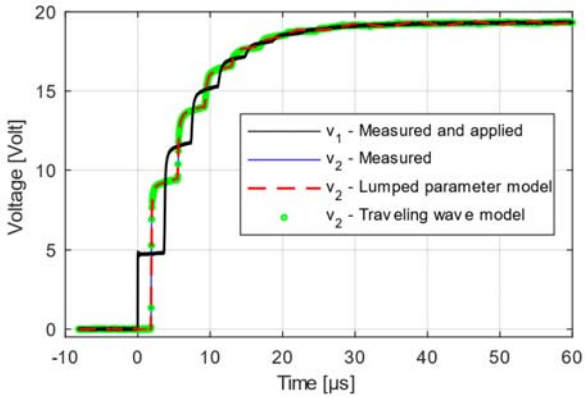

Fig. 10a. Measured and simulated voltage. Far end open.

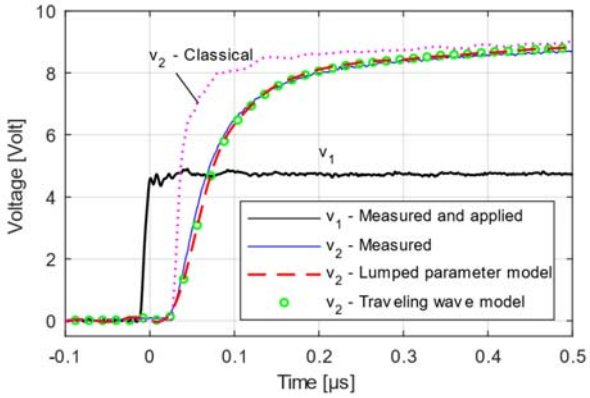

Fig. 10b. Zoomed view of fig. 10a. Response $v_2(t)$ shifted 1.8 µs.

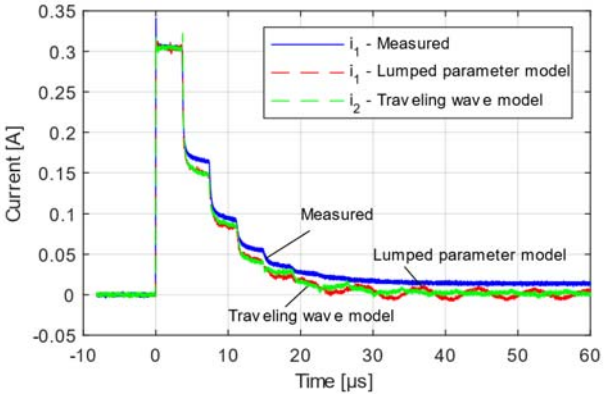

Fig. 10c. Near end current response.

C. Loaded End

The same comparison was performed when the cable far end was loaded with a 50 Ω resistor. Figs. 11a and 11b show that the lumped parameter model and the traveling wave model reproduce the measured voltage wave shape with excellent agreement. The deviation by the classical method in Fig. 11b is similar as for the open end case (Fig. 10b), giving much too little damping of the wave front.

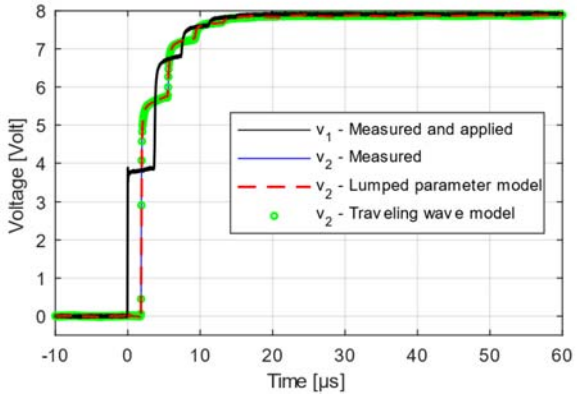

Fig. 11a. Measured and simulated voltage. Far end loaded by 50 Ω.

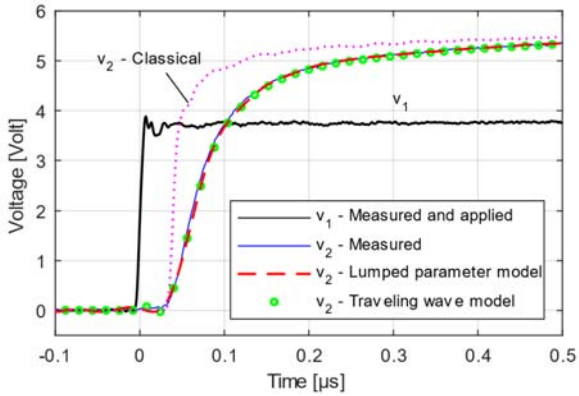

Fig. 11b. Zoomed view of fig. 9a. Response $v_2(t)$ shifted 1.8 μs.

D. Open End Response With Use of Amplifier

The 50 Ω internal resistor in the function generator (Fig. 9) results in a damping of the cable transient waveforms which can mask the cable damping characteristics. This damping effect was reduced in a second set of experiments by placing a wide-band amplifier between the function generator and the cable near end.

Fig. 12 shows the measured responses with the cable far end unloaded, using the lumped parameter model and the traveling wave model. The measured waveform is still well reproduced by the model, including the dominant frequency component of about 129 kHz. The front steepness of the applied voltage is lower than in the previous two examples, due to the limited frequency range of the amplifier. A similar accuracy was achieved with the far cable end loaded with 50 Ω.

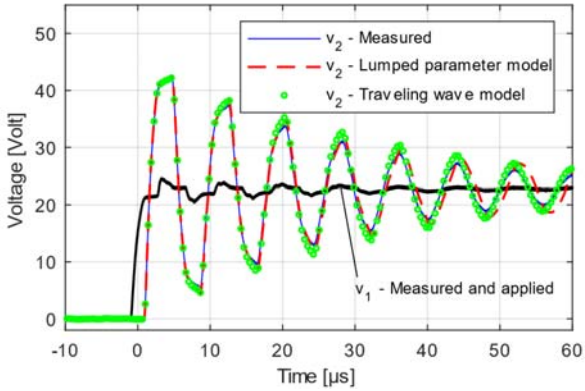

Fig. 12. Use of amplifier with far end open.

X. Result With Alternative Cable Lengths

Fig. 13 shows a simulation of the cable far end unit step response, with the far end open. The simulation was performed using the traveling wave model with parameters calculated for three alternative lengths: 125 m, 250 m and 500 m. It can be observed that all models produce smooth responses.

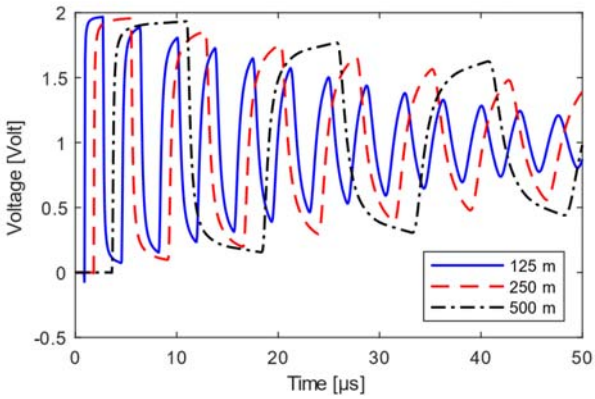

Fig. 13. Step voltage response at open far end with alternative cable lengths.

XI. Discussion

A. Oscillations in Characteristic Admittance

It was shown in Section VII.E (Fig. 8b) that the calculated characteristic admittance Y_C has spurious oscillations at high frequencies. Such oscillations can lead to difficulties in calculating a low-order rational function approximation of Y_C. As a remedy one may use a real-valued, constant Y_C as indicated by the dashed line in Fig. 8b. This option was found to give a fully adequate representation at very high frequencies

(not shown in the paper).

B. Lumped Parameter Modeling With Alternative Cable Lengths

The calculation of p.u.l. parameters makes it possible to change the length of the traveling wave model, as demonstrated in Section X. The change in length can also be applied to the lumped parameter model by calculating the terminal admittance matrix via (20a) and (20b). Such approach was already used in [13].

C. On-Site Model Validation

It is important to assess the model accuracy in the time domain because it is difficult to predict how model inaccuracies in the frequency domain translates into errors in the time domain. Such validation can performed at the cable near end by measuring the current response due to a steep fronted voltage application, similar to the comparison in Fig. 10c. Time domain validation is not possible if the model has been calculated for a length that differs from that of the actual cable.

XII. Conclusion

A measurement-based method is proposed for characterizing the terminal behavior of screened cables at high frequencies. Using three one-sided voltage transfer measurements, the 2×2 terminal admittance matrix is calculated with the use of a swept rational model for removal of sign ambiguity of the off-diagonal element. From the terminal admittance matrix is extracted two alternative models, a high-order lumped-parameter model and a low-order traveling wave model. Both model types are applicable in EMTP-type simulation programs. Models for other cable lengths can be calculated from the given measurement.

Application to a 252 m 150 mm^2 screened cable showed that the method gives models that can reproduce sub-microsecond damping effects of fast wave fronts with high accuracy whereas a classical modeling method based on skin effect formulae gives much too little damping. The proposed method is therefore suitable for modeling cables that need to be represented accurately at very high frequencies, for instance when predicting winding stresses in motors that are fed from power electronic switch-mode converters via a cable. One key advantage of the proposed method is that it requires measurements at one cable end only, thereby making it applicable to installed cables.

XIII. Acknowledgement

The author appreciates fruitful discussions with Henrik Strand and the laboratory support from Oddgeir Rokseth, both SINTEF Energy Research. Equinor is thanked for providing the cable sample used in this work.

References

[1] CIGRE Technical Brochure 577A, “Electrical transient interaction between transformers and the power system. Part 1 – Expertise”, CIGRE JWG A2/C4.39, April 2014.

[2] P. G. McLaren and M. H. Abdel-Rahman, “Modeling of large AC motor coils for steep-fronted surge studies, ” *IEEE Trans. Industry Applications*, vol. 24, no. 3, pp. 422-426, May-June 1988.

[3] Y. Tang, “Analysis of steep-fronted voltage distribution and turn insulation failure in inverter-fed form-wound AC motor”, *IEEE Trans. Industry Applications*, vol. 34, no. 5, pp. 1088-1096, Sept.-Oct. 1998.

[4] L. Marti, “Simulation of transients in underground cables with frequency-dependent modal transformation matrices,” *IEEE Trans. Power Delivery,* vol. 3, no. 3, pp. 1099-1110, July 1988.

[5] A. Morched, B. Gustavsen, and M. Tartibi, “A universal model for accurate calculation of electromagnetic transients on overhead lines and underground cables”, *IEEE Trans. Power Delivery*, vol. 14, no. 3, pp. 1032-1038, July 1999.

[6] A. Ametani, “A general formulation of impedance and admittance of cables,” *IEEE Trans. Power Apparatus and Systems*, vol. PAS-99, no. 3, pp. 902-910, May 1980.

[7] L.M. Wedepohl and D.J. Wilcox, “Transient analysis of underground power-transmission systems. System-model and wave-propagation characteristics,” *Proc. IEE*, vol. 120, no. 2, pp. 253-260, Feb. 1973.

[8] U.R. Patel and P. Triverio, “Accurate impedance calculation for underground and submarine power cables using MoM-SO and a multilayer ground model,” *IEEE Trans. Power Delivery*, vol. 31, no. 3, pp. 1233-1241, June 2016.

[9] Y. Yin and H. W. Dommel, “Calculation of frequency-dependent impedances of underground power cables with finite element method,” *IEEE Trans. Magnetics,* vol. 25, no. 4, pp. 3025-3027, July 1989.

[10] B. Gustavsen, A. Bruaset, J. Bremnes, and A. Hassel, ”A finite element approach for calculating electrical parameters of umbilical cables”, *IEEE Trans. Power Delivery,* vol. 24, no. 4, pp. 2375-2384, Oct. 2009.

[11] J. J. Guo, L. Zhang, C. Xu and S. A. Boggs, “High frequency attenuation in transmission class solid dielectric cable,” *IEEE Trans. Power Delivery*, vol. 23, no. 4, pp. 1713-1719, Oct. 2008.

[12] I. Stevanović, B. Wunsch, G. L. Madonna and S. Skibin, “High-frequency behavioral multiconductor cable modeling for EMI simulations in power electronics,” *IEEE Trans. Industrial Informatics*, vol. 10, no. 2, pp. 1392-1400, May 2014.

[13] B. Wunsch, I. Stevanović and S. Skibin, “Length-scalable multiconductor cable modeling for EMI simulations in power electronics," *IEEE Trans. Power Electronics*, vol. 32, no. 3, pp. 1908-1916, March 2017.

[14] B. Gustavsen, “Wide band modeling of power transformers”, *IEEE Trans. Power Delivery*, vol. 19, no. 1, pp. 414-422, Jan. 2004.

[15] B. Gustavsen, “Study of transformer resonant overvoltages caused by cable-transformer high-frequency interaction”, *IEEE Trans. Power Delivery*, vol. 25, no. 2, pp. 770-779, April 2010.

[16] B. Gustavsen, B. Tandstad, "Wide band modeling of a 45-MVA generator step-up transformer for network interaction studies", *Electric Power Systems Research*, vol.142, pp. 47-57, Jan. 2017.

[17] B. Gustavsen, and A. Semlyen, “Rational approximation of frequency domain responses by vector fitting”, *IEEE Trans. Power Delivery*, vol. 14, no. 3, pp. 1052-1061, July 1999.

[18] B. Gustavsen, and A. Semlyen, “Enforcing passivity for admittance matrices approximated by rational functions”, *IEEE Trans. Power Systems,* vol. 16, no. 1, pp. 97-104, Feb. 2001.

[19] B. Gustavsen, “Passivity enforcement by residue perturbation via constrained non-negative least squares”, *IEEE Trans. Power Delivery*, vol. 36, no. 5, pp. 2758-2767, October 2021.

[20] B. Gustavsen, “Computer code for rational approximation of frequency dependent admittance matrices”, *IEEE Trans. Power Delivery*, vol. 17, no. 4, pp. 1093-1098, October 2002.

[21] B. Gustavsen and H.M.J. De Silva, “Inclusion of rational models in an electromagnetic transients program – Y-parameters, Z-parameters, S-parameters, transfer functions”, *IEEE Trans. Power Delivery*, vol. 28, no. 2, pp. 1164-1174, April 2013.

[22] A. Semlyen and B. Gustavsen, “Phase domain transmission line modeling with enforcement of symmetry via the propagated characteristic admittance matrix”, *IEEE Trans. Power Delivery*, vol. 27, no. 2, pp. 626-631, April 2012.

[23] S. Grivet-Talocia and B. Gustavsen, *Passive Macromodeling*. Wiley Hoboken NJ USA Dec. 2015.

[24] B. Gustavsen, “Panel session on data for modeling system transients: Insulated cables”, *Proc*. IEEE PES Winter Meeting, vol. 2, pp. 718-723, 2001.

[25] S.A. Schelkunoff, “The electromagnetic theory of coaxial transmission lines and cylindrical shields”, *Bell System Technical Journal*, vol. 13, pp. 532-579, 1934.

BIOGRAPHY

Bjørn Gustavsen (M'94–SM'2003–F'2014) was born in Norway in 1965. He received the M.Sc. degree and the Dr. Ing. degree in Electrical Engineering from the Norwegian Institute of Technology in Trondheim, Norway, in 1989 and 1993, respectively. Since 1994 he has been working at SINTEF Energy Research, currently as Chief Research Scientist. He is also an adjunct Professor at NTNU, since 2020. His interests include simulation of electromagnetic transients and modeling of frequency dependent effects. He spent 1996 as a Visiting Researcher at the University of Toronto, Canada, and the summer of 1998 at the Manitoba HVDC Research Centre, Winnipeg, Canada. He was Marie Curie Fellow at the University of Stuttgart, Germany, August 2001–August 2002.